Proceedings of the 21st ICSMGE, Vienna, Austria, 14 – 19 June 2026. Pistrol, Adam & Schweiger (eds.)
Published by: ÖGG, Austrian Society for Geomechanics, Salzburg, Austria, ISBN 978-3-9503898-4-5
https://doi.org/10.53243/ICSMGE2026-703

Complementarities of *in-situ* (CPTu, DCPT, Cyclic Pressuremeter) and laboratory tests for the study of earthquake-induced soil liquefaction (alluvial context, Croatia).

Denis Moiriat, Badara Soumounou
SCAN Department, French Authority for Nuclear Safety and Radiation Protection (ASNR), France, denis.moiriat@asnr.fr

Sonia Fanelli, Philippe Reiffsteck
GERS Department, University G. Eiffel, France

Miguel Navarrete, Tuan-Anh Luong
Research Department, Sol Solution, France

Josipa Maslač Soldo, Branko Kordic
HGI-CGS, Croatian Geological Survey, Croatia

ABSTRACT: This work presents an application of various geotechnical tests on one alluvial site with a lot of occurrences of sand blows following the Petrinja Earthquake (M_w ~ 6.3-6.4) which stroke Croatia in Dec. 2020. The combination of more classical tests (CPTu, cyclic laboratory tests) and innovative tests such as the instrumented Dynamic Cone Penetrometer test (DCPT) or the Cycle Pressuremeter Test, enable detailed exploration of site conditions and outlines some specific advantages of these new tests for the study of earthquake-induced soil liquefaction from *in-situ* tests and for soil characterization more broadly. Thanks to their repeatability and their new sensors, the instrumented DCPT provides fine information with depth regarding the state of soils or their fabric and, coupled with CPT, makes it possible to define a fairly precise geotechnical model. Cyclic Pressuremeter test also turns out to be a relevant tool to compare notably the liquefaction behavior of the soil measured in laboratory that estimated under *in-situ* conditions. This combination of classical and innovative tests also provides a fairly reliable diagnosis of the liquefiable layers that caused sand blows at the surface in this specific context of sand point bars buried below a silt cover.

KEYWORDS: soil liquefaction, CPTu, DCPT, Cyclic Pressuremeter Test, cyclic laboratory tests, point bar, sand blow, Croatia

1 INTRODUCTION

In intraplate context, the alluvial plain of Petrinja-Sisak (Croatia) is located at the junction between the southwest part of the Pannonian basin and the north of the Internal Dinarides. Liquefaction occurrences were observed in this area in 1909 during the "Kupa Valley earthquake" (mainshock Ms ~ 5.75-6) (Herak & Herak 2010) and, more recently, during the Petrinja earthquake in Dec. 2020 (mainshock M_w ~ 6.3-6.4) which occurred along the same fault system and generated numerous sand blows along the Kupa, Sava and Glina rivers in unconsolidated Holocene alluvial sediments (Baise et al. 2022).

This high susceptibility of soils to liquefy, based on historical and geological considerations (Kramer 1996), and easy access to liquefied sites in this alluvial plain provide an opportunity to test innovative geotechnical devices and calibrate them against more conventional tools such as the Cone Penetration Test (CPT) or Standard Penetration Test (SPT) traditionally used in geotechnics to study liquefaction risk.

Between 2022 and 2024, three campaigns of geotechnical and geophysical investigations, detailed hereafter, were led at different sites close to the riverbanks of the Kupa river with sand blows and lateral spreads which occurred in Dec. 2020. Six trenches were also excavated to observe and sample the injections of sandy dykes at depth and located below the sand blows at the surface.

From the ground surface, the alluvial sediments of the Kupa river, water-saturated by the river aquifer, correspond to about 3 m thick clayey silts (Unit 1) overlying sandy layers at least 3 m thick (Unit 2), followed by gravels and coarse sands (Unit 3) underneath. Previous results mainly based on sieve analysis have shown that all sand blows at the surface or their sand dykes at depth correspond to poorly graded sand with silt (SP-SM) or silty sand (SM) and originate from sand point bars buried under the silty cover (Unit 1) between 3 and 6 m of depth (Luong et al. 2022).

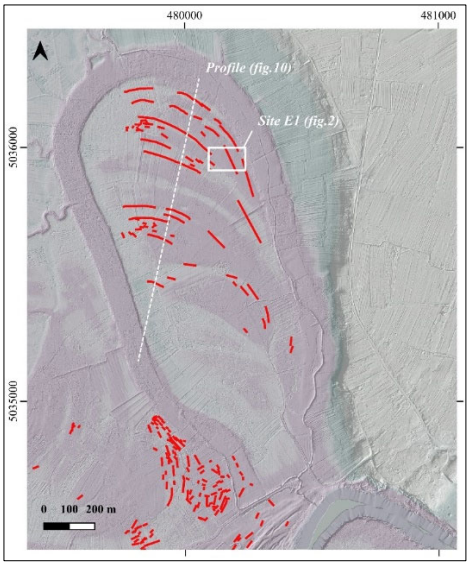

Figure 1. Location of site E1 and lines of sand blows mapped just after the Petrinja earthquake in Dec. 2020 by drone (red color).

This work outlines the contribution made by cross-referencing various geotechnical investigations carried out in 2024 on one site called "site E1", located on the eastern edge of an ancient meander (Figure 1). Its convex part presents clearly well-marked lines of sand blows with typical arched morphologies reflecting the morphology and the accretion process of the underlying sandy deposits (scroll bars) in the meander (Valkaniotis et al. 2024)

2 TYPES OF INVESTIGATIONS ON SITE E1

Within this site E1 underlined by a flat topography (mean altitude at 99 m absl), geological drillings and different geotechnical soundings laid out in perpendicular lines to the edge of the meander (Figure 2) and up to a depth of 15 m. which include the following for the building of geotechnical model in particular:

- 4 static Cone Penetration Tests with pore pressure measurement (CPTu) chosen for their robustness to identify all liquefiable layers through the measured cone resistance (q_c) and the sleeve friction resistance (f_s) (Robertson & Cabal 2022)
- 19 instrumented Dynamic Cone Penetrometers Tests (DCPT), suitable for all soils unlike CPT, and selected for their simplicity and their repeatability which allows fine prospection of soils with a large number of soundings at a much lower cost than CPT, in order to characterize soil spatial variability. Much more robust and accurate than Standard Penetration Test (SPT), it provides both the dynamic cone resistance (q_d) and thanks to new version incorporating new sensors (Benz Navarrete and al. 2022), the compressional wave velocity (V_p). As a result, an estimation of the shear wave velocity (V_s) with an assumption on the Poisson ratio is then possible at any depth.
- 3 core drilling for observations and identification tests from samples (sieve analysis and plasticity index for fine soils mainly).

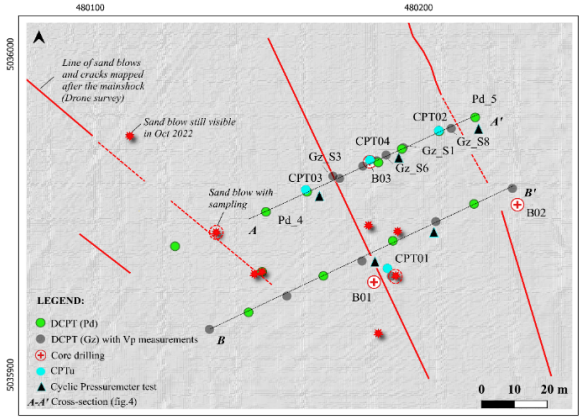

Figure 2. Location of *in-situ* investigations at site E1 and liquefaction occurrences observed at the surface after the mainshock (red color).

In parallel and from samples of sand dykes identified on a site very close to site E1 (blue curve in Figure 3), twelve cyclic triaxial tests were performed in laboratory in saturated and undrained conditions, enabled the definition of liquefaction resistance curves showing the cyclic resistance (CRR) or the excess pore pressure ratio (r_u) as a function of the number of cycles at liquefaction (N_L) and for different ranges of density index (I_D).

To complete these liquefaction curves, especially at low I_D difficult to achieve with triaxial tests, 5 cyclic pressuremeter tests were carried out on the field between 3 and 5 m of depth using Menard pressuremeter in prebored holes (Figure 2). Several sequences of sinusoidal cycles of varying amplitudes were then applied successively to observe the reduction in volumic strain accumulation as a function of the number of cycles until it reaches liquefaction at N_L (Reiffsteck et al. 2013; Karagiannopoulos et al. 2022; ISO 2023).

3 OVERVIEW OF THE STUDY METHODOLOGY

This work breaks down into five stages, from the characterization of soils and geometries to the identification of liquefiable layers, and underlining for each stage the complementary of different geotechnical tests:

Thanks to new data acquired in 2024, the first stage has been to specify the previous 2D geotechnical model based mainly on instrumented DCPT and core drillings (cross-section B-B' in Figure 2) and presented in Luong et al. 2022) through a new cross-section A-A'(Figure 2).

The second stage looks at all the conditions prone to liquefaction and focuses on relevant indicators related to the state or fabric of soils such as the shear wave velocity (V_s), the high permeability contrasts (k_v) or the I_D values for coarse-grained soils. As all the geotechnical soundings were implemented in Oct. 2022 and March 2024, we bear in mind that the soil condition is no longer the one which existed before or just after the earthquake in Dec. 2020 and that the estimated I_D values especially, if representative enough, reflect one state of compactness after a long period without ground shaking since the 2020 earthquake sequence.

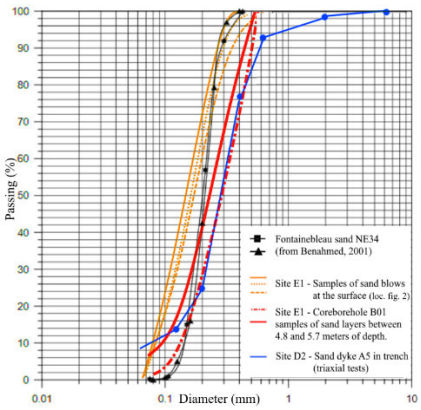

Figure 3. Grain sizes of studied sands

The third- and fourth stages deal with the identification of layers which would be liquefied in case of a new earthquake similar to the 2020 Petrinja earthquake, in using the simplified approach detailed in Youd et al. (2001) by comparing the soil resistance at liquefaction (CRR) and the seismic demand (Cyclic Strength Ratio or CSR) approached by the equation of Seed & Idriss 1971. Despite the strong limitations of this method (Pyke 2003; Semple 2013), notably because earthquake information is limited to some parameters without any consideration for the ground motion frequency, this first approach nevertheless allows us to identify the most plausible sources of liquefied materials and then to discuss the possible mechanisms for the occurrence of sand blows at the surface in this alluvial context. A numerical effective-stress analysis would have been a more rigorous approach, but this one requires the calibration of parameters used in the model.

The last and fifth stage cross-references the results of liquefaction triggering deduced from *in-situ* tests and laboratory tests with the updated geotechnical model before discussing them.

4 RESULTS

4.1 *Updated geotechnical model*

Thanks to clear variations of f_s and q_c between fine soils and sands (limit between Unit 1 and Unit 2) or between sands and gravels (limit between Unit 2 and Unit 3), the lithological limits between each unit can be specified using CPTu and then extended using dynamic cone penetrometers (DCPT) profiles.

The vertical variations (Figure 4). of these limits reveal wide undulations with a horizontal length about 30 m which correspond to geomorphological features of sandy scroll bars (Unit 2) buried under the silt cover (Unit 1) as described in Francisković-Bilinski et al. 2011 and in consistency with the cross-section B-B' presented in Luong et al. 2022.

The combination between CPTu through the Soil Behaviour Type (SBT) values and DCPT through q_d variations also allows to describe in a greater detail the stratigraphy:

- Unit 1 presents a general decrease of q_c or q_d (ranging from 3.5 MPa to less than 1 MPa) and can be subdivided in superficial layer of clayey silt (Unit 1A) and a main heterogeneous layer including organic and clayey soils alternating with sandy and silty mixtures (Unit 1B) underlined by a sand content increase with depth up to 50 % (sieve analysis results).
- Unit 2 can be also divided into two layers with a layer of silty sands (Unit 2A) and a layer of sands much less silty. The change from Unit 1 to Unit 2 is generally underlined by an increase of q_c or q_d and then values steadily continue to increase with the depth until reaching 5 and 8 MPa at the bottom of Unit 2.
- Unit 3 comprises at least 2 layers, one with dense sands and including gravel interbeds (Unit 3A), one other beginning with a layer of fine soils and then more and more gravelly with high q_c or q_d (exceeding 5-6 MPa).

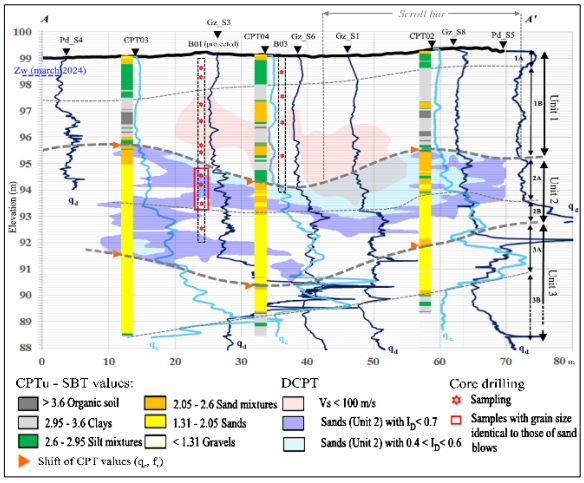

Figure 4. Geotechnical. model along profile A-A' (loc. in fig.2)

4.2 *Site conditions prone to liquefaction*

In this part, three indicators are looked at: the shear wave velocity (V_s), the *in-situ* I_D for the sandy soils of Unit 2 and the vertical permeability (k_v) of different layers.

The V_s values presented in Figure 5 are either derived from DCPT for all soils or estimated only for the Holocene sands of Unit 2 according to the V_s relationships developed by Robertson (2009) from CPTu and valid for most Holocene to Pleistocene-age deposits but less reliable for fine-grained soils. All those Vs values are consistent with both the measured V_s from MASW profiles (Multiple Analysis of Surface Waves) carried out in Sept. 2023 along the B-B' cross-section (loc. Figure 2) and the V_s range for points bars deposits (Morrison 2017) and surface sediments in general with $V_s \leq 300$ m/s (Lee 2010). In particular, the lowest V_s values (< 100 m/s) are distributed in Unit 1B and Unit 2A (main areas in Figure 4) and also fit with the lowest values of q_c or q_d. These areas of very soft material also seem to be distributed above and between two scroll bars (Figure 4).

The *in-situ* I_D derived from DCPT results using a correlation ($R^2 > 0.9$) proposed by Retamales (2022) from a fine liquefiable sand of Fontainebleau NE34 (France) which presents a similar grain size distribution to that of sandy blows on site E1 (Figure 3):

$$I_D = 0.335.Ln\,(q_{d;n}) + 0.237 \quad (1)$$

With qd_n the normalized penetration resistance given by:

$$q_{d;n}=q_d.\left(\frac{p_a}{\sigma'_v}\right)^{0.5} \text{ and } \left(\frac{p_a}{\sigma'_v}\right)^{0.5} \leq 2.5 \quad (2)$$

With q_d the penetration resistance value from DCPT; p_a the atmospheric pressure; and σ'_v the vertical effective stress.

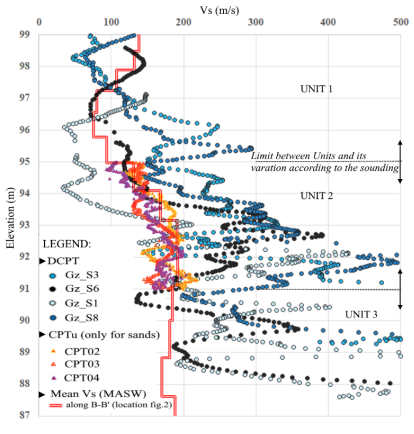

Figure 5. Shear wave velocity (V_s) versus depth for the geotechnical soundings along the cross-section A-A' (loc. in fig.2)

The distribution of *in-situ* I_D in Unit 2 is presented in Figure 4 and pinpoints low compactness of sands preferentially at the top of a scroll bar in Unit 2A and, more rarely, in some zones in-depth in Unit 2B where the sands tend to be denser. This vertical distribution in Unit 2 presumably reflects the depositional history and soil fabric of these sandy bars but might also be evidence of sand remobilization linked to past shaking in this environment of loose to very loose sediments.

From the hydraulic point of view, the groundwater level was reached during the drilling in 2024 around 2 m of depth in Unit 1B to steady at less than 1 m of depth a few hours later. In this unit, the vertical permeabilities (k_v). derived from CPTu (Robertson & Cabal 2022). are low enough and present strong contrasts (k_v between 10^{-10} and 10^{-6} m/s). In Unit 2, the permeabilities are lower in Unit 2A ($k_v < 10^{-5}$ m/s) than in Unit 2B ($k_v < 10^{-4}$ m/s) which also overlies a more permeable Unit 3A ($k_v < 10^{-3}$ m/s). As a result, the hydraulic context appears much more favorable for the water pressure build-up during ground shaking in Unit 1B and in Unit 2A.

4.3 *Triggering liquefaction from CPTu*

In this evaluation and given the flat topography ($K_\alpha = 1$), the Safety Factor (SF), indicating a triggering liquefaction if SF < 1, is classically defined by:

$$SF = \frac{CRR_{7.5}}{CSR_M}.MSF.K_\sigma \quad (3)$$

With $CRR_{7.5}$ is the normalized cyclic soil resistance for a magnitude M_w of 7.5; CSR_M the normalized mean stress generated by the earthquake of magnitude M_w; MSF a corrective magnitude factor depending on M_w and considered in this study equals to boundaries MSF_{min} and MSF_{max} recommended in the method for an earthquake with $M_w < 7{,}5$ (Youd et al. 2001) in order to cover the uncertainty associated with this parameter; and K_σ an additional corrective factor linked to the effective confining pressure as the CSR does not vary linearly with depth.

In the equation of Seed & Idriss 1971 for the determination of CSR, the peak ground acceleration (PGA) at the surface for the mainshock is set at a plausible minima mean value of 0.2 g, based on the one hand, on some recordings from accelerometers installed in the area of the city of Zagreb located approximately 50 km north of Petrinja and, on the other hand, on our own estimates from ground motion prediction equation depending on the uncertain value of V_s in the first thirty meters ($V_{s,30}$).

In other respects, several tests with low values of K_σ (up to 0.8 for sands with low I_D of 0.4 to 0.6 in particular) indicate that, in this context of unconsolidated sediments at low depths, this parameter can be taken equal to 1 as a first approximation (Figure 6).

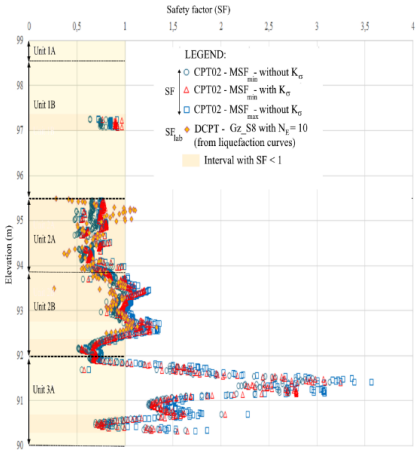

Figure 6. PGA = 0.2g - Comparison of Safety Factor (SF) values from CPT02 and DCPT Gz_S8 (loc. in Fig. 2).

For a PGA of 0.2 g, the results confirm that the main intervals with SF < 1 are located mainly in sandy Unit 2A and Unit 2B and more locally in sand mixtures of Unit 1B and sands layers of Unit 3A (example with CPT02 in Figure 6). Almost all Unit 2 is involved at this PGA with a thickness of liquefiable sands upper than 3 m, which might justify the significant volumes of ejected sands at the surface in 2020 with thicknesses in the heart of sand blows often outreaching 20-30 cm (Figure 7).

4.4 *Liquefaction study from laboratory and cyclic pressuremeter tests*

4.4.1 *Liquefaction curves*

Laboratory tests to simulate seismic liquefaction were performed in soil samples using a triaxial apparatus. Beforehand, the different samples were water saturated and isotopically reconsolidated to the desired value of I_D. Each cyclic test was carried out at a confining pressure of 100 KPa (~5 m of depth) and in applying an identical sinusoidal deviator stress at a frequency of 0.03 Hz until liquefaction. Different values of loading CRR (0.1 - 0.3) and I_D (0.5 - 0.9) have been studied in order to get the number of cycles at liquefaction (N_L) for set values of CRR and I_D.

The liquefaction criteria used in this laboratory study to estimate N_L is mainly based on the value of excess pore pressure ratio (r_u), defined as the ratio between the variation of water pressure and the confining pressure, and which equals to 1 at liquefaction. All the triaxial tests reveal a transition phase (r_u ~ 0.7 to 0.8) beyond which the soil systematically liquefies and collapses (r_u = 1). This abrupt loss of rigidity would result in a change in state from solid to liquid.

The sufficient number of tests with I_D between 0.6 and 0.8 is then used to draw the curves CRR = f (N_L) with a fairly good correlation ($R^2 > 0.85$) for two ranges of I_D (curves C1 and C2 presented in Figure 8):

$$CRR = a.N_L^{-b} \quad (4)$$

With a between 0.23 to 0.31 according to the I_D value and b another coefficient equals to 0.159 in consistence with the bibliography for same kind of materials and tests (Chattaraj & Sengupta 2016; Serratrice 2016).

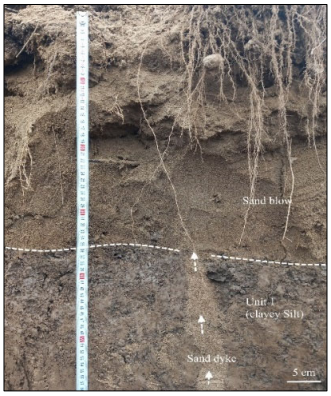

Figure 7. Example of sand dyke below its sand blow linked to the 2020 Petrinja earthquake ((Lat 45.471819°; Long 16.225298°)

The results of *in-situ* cyclic pressuremeter tests in Unit 2A are also presented in Figure 8. At equivalent I_D ranges between 0.6 and 0.8, the results lined up on the C1 and C2 curves deduced from laboratory tests. They therefore confirm the consistency of the liquefaction curves deduced from the laboratory tests and also allow us to consider, on the other hand, that the liquefaction behavior of the soil observed in the laboratory is fairly representative of that under *in-situ* conditions. In addition, the cyclic pressuremeter provides information on intact soils at very low I_D (0.3 to 0.5) what is difficult to get in laboratory (Figure 8).

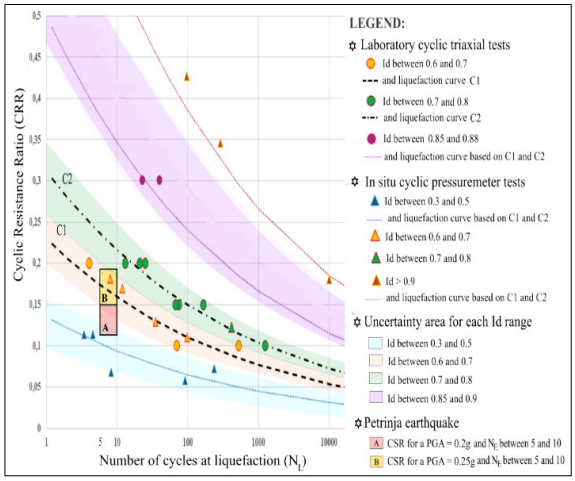

Figure 8. Liquefaction curves for sands from triaxial tests (samples at σ'_3 = 100 KPa) and cyclic pressuremeter tests (Unit 2A, loc. in fig. 2).

In order to complete the results for the other I_D ranges ($I_D < 0.6$ or $I_D > 0.8$), liquefaction curves have been then looked for with the same b exponent value and variable a value adjusted to test results (triaxial and pressuremeter tests) and depending, as a result, on the I_D value according to the equation:

$$a = 0.0427.e^{2.8784.I_D} \ (R^2 = 0.9429) \quad (5)$$

Each curve has been drawn with its uncertainty range framing the different results (Figure 8).

4.4.2 *Triggering liquefaction from liquefaction curves*

With all the curves whatever the I_D values for sands, it is then possible to compare the soil resistance at liquefaction (CRR) and the seismic demand (CSR), without the need to include a corrective magnitude factor (MSF) and with a number of cycles at liquefaction (N_L) corresponding to the number of cycles of earthquake. This latter can be approximated with an equivalent number of uniform stress cycles (N_E) which can be computed from different earthquake time series (Idriss & Boulanger 2008) or throughout empirical correlations as N_E is function of the M_w magnitude, PGA and distance to the fault surface (Green & Terri 2005; Hancock & Bommer 2005). As no recording of the mainshock is available near the areas studied along the Kupa river, we have considered minimum plausible N_E values for a magnitude M_w of 6.3 according to the bibliography (Lasley et al. 2016) with N_E between 5 ($N_{E,min}$) and 10 ($N_{E,max}$) for a hypocentral distance around 10 km (site E1 is located around 7.5 km from the epicenter) and for a magnitude M_w of 5.5.

In this way, we can define a safety factor from liquefaction curves (SF_{lab}) by:

$$SF_{lab} = \frac{a.N_E{}^{-b}}{CSR_M} \quad (6)$$

With SF_{lab} depending only on both PGA and N_E for the earthquake and I_D value for sand estimated from DCPT. Of note are underlying limitations to applying this formula as liquefaction curves have been defined only at 100 kPa and for one specific of grain size distribution curve (Figure 3). In addition, the CRR from triaxial tests usually require correction to be representative of field conditions, around 0.55-0.70 for clean sands with I_D range 0.4-0.85 (Kokusho 2016), but difficult to calibrate accurately as part of this study. Given moreover that CRR from *in-situ* cyclic pressuremeter tests is equivalent of CRR from laboratory tests for same I_D and N_L (Figure 8), this corrective factor has been taken to be equal to 1 in first approximation for the purposes of our study.

One example of SF_{lab} is presented Figure 6 to compare with SF values from CPTu in sands of Unit 2. The SF_{lab} are well in line with the SF values from CPTu and make it possible to include these results in the screening of liquefiable layers. This consistency between laboratory and *in-situ* results also provides in return a reasonable degree of confidence about the considered estimation of *in-situ* I_D from DCPT.

In Figure 8, the useful characteristics of Petrinja earthquake (CSR and N_E) are plotted and located in the vicinity of C1 curve. That would reveal that the sands of Unit 2 with $I_D \leq 0.6$ would have been easily liquefied for a PGA of 0.2 g and those with an $0.6 \leq I_D < 0.8$ could have been affected if PGA reached 0.25 g. The overall results are discussed hereafter.

4.5 *Cross-referencing SF and SF_{lab} results with the geotechnical model - Discussion*

In Figure 9, the SF and SF_{lab} results for a PGA of 0.2 g are plotted with their respective uncertainties on the geotechnical model mainly based on CPT and DCPT results.

This overview at 0.2g firstly confirms that all Unit 2 could have been concerned by the liquefaction phenomena, either continuously on the whole thickness (ex. CPT03, Gz_S3 in Figure 9) or in specific layers (ex. CPT04, Gz S6 in Figure 9). Secondly, it underlines that the total thickness of liquefiable sandy layers in Unit 2 seems to be more significant at the top of scroll bars where the sands present the lowest I_D in Unit 2 and where the thickness of Unit 1 is less. In addition, the main lines of sand blows at the surface on this profile A-A' (loc. in Figure 2) seem to be located above these areas (Figure 9).

Unit 1B also includes some liquefiable lenses of sand and silt mixtures that are too thin however to explain the significant sand volumes observed at the surface. In addition, their granular sizes don't match with those of sand blows. Unit 3A also presents some thin and rare sandy liquefiable layers in-depth which can be ruled out for the same conclusions as Unit 1B and also given the high permeabilities on the unit scale not conducive to water overpressure.

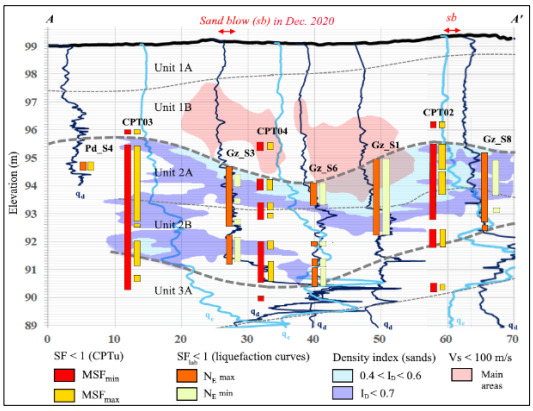

Figure 9. Identification of liquefiable layers for a PGA of 0.2 g along cross-section A-A' (location in fig.2)

This preferential location of sand blows above top of scroll bars can be enlightened on a wider meander scale with a profile sub-perpendicular to the lines of sand blows (Figure 1) and for which the slight topographical variations can be highlighted thank to a high-resolution Digital Elevation Model (Figure 10).

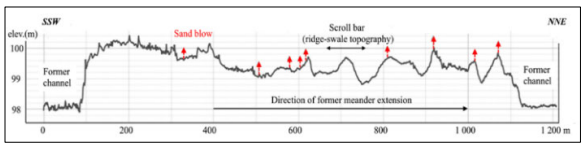

Figure 10. Former meander of Kupa river - Link between scroll bars and sand blows at the surface (loc. in fig. 1)

According to the E1 site results, this preferential location of sand blows just below top of scroll bars could be linked in part to the lower compactness of sandy soils in these specific geomorphological areas. However this hypothesis has yet to be confirmed by a detailed literature review on the depositional history of sand point bars in general.

By the way, the role of Unit 1B in the process of emergence of sand blows hasn't still been well clarified. Unit 1B includes indeed areas with very low mechanical strength or V_s, in particular the zones with $V_s < 100$ m/s (Figure 9) which could have enabled more easily the rising sand up to the surface. In other sites, Electrical Resistivity Tomography (ERT) profiles have highlighted the presence of a silty layer with $q_d > 5$ MPa at the bottom of Unit 1 preventing the sand blows emerging. In addition and more locally for the site E1, the upward water pressure of the aquifer in Unit 1 which presumably existed before the earthquake (aquifer slightly artesian in Oct. 2022 and March 2024) could also have facilitated the process of ejection toward the surface. Nevertheless this water condition has not been observed on other sites along the Kupa river.

Accordingly, the process of the occurrence of sand blows mainly depends on the available thickness of liquefiable sand in Unit 2 on the one hand (ejecta demand), and properties of cohesive Unit 1 on the other hand, both its thickness and its mechanical strength which oppose to ejecta demand. This result is in line with the model of the simplified procedure to estimate

ejecta potential developed by Hutabarat & Bray (2021) to capture these two competing effects.

5 CONCLUSIONS

This short study on one alluvial site with susceptible soils to liquefy presents the benefits of applying new geotechnical tests, DCPT and cyclic pressuremeter test especially and their complementarity with more classical tests such as CPTu or triaxial laboratory tests for the study of earthquake-induced soil liquefaction.

Thanks to their repeatability and their new sensors, the instrumented DCPT provides a lot of detailed information with depth regarding the state of soils or their fabric (I_D or V_s) in consistency with other measurements (MASW) regarding the estimations of V_s more especially. Paired with CPT, they make it possible to define a fairly precise geotechnical model in good adequation with the geological model in this alluvial context of sand points bars.

Cyclic pressuremeter also turns out to be a particularly relevant tool for linking *in-situ* and laboratory results. These tests, performed *in-situ* on intact soils, notably allows both to check the validity of liquefaction curves defined from laboratory tests on reconstituted sand samples at different I_D and to complete them for low ranges of I_D in particular, which is difficult to obtain from laboratory tests.

Despite the strong limitations of the simplified method, the consistency of the results from *in-situ* and laboratory tests tends to confirm the robustness of the diagnosis for the identification of liquefiable layers that caused sand blows in this study case with a clearly distinct liquefiable layer in Dec. 2020 located just below a non-liquefiable cohesive layer. However, it is by no means certain that this consistency of results between *in-situ* and laboratory tests will be found in other geological contexts with much more lithological heterogeneities for instance (sand and gravel lenses) or fine alternations (interbedded sands and fine-grained soils).

6 ACKNOWLEDGEMENTS

We thank the Croatian Geological Survey (HGI-CGS) for their invaluable support during all the geotechnical and geophysical investigations on the field.

7 REFERENCES

Baize, S., Amoroso, S., Belic, et al., 2022. Environmental effects and seismogenic source characterization of the December 2020 earthquake sequence near Petrinja (Croatia), *Geophysical Journal International*, Vol. 230, 1394–1418.

Benahmed, N. 2001. Comportement mécanique d'un sable sous cisaillement monotone et cyclique : application aux phénomènes de liquéfaction et de mobilité Cyclique. Ph. D. Thesis, *Ecole Nationale des Pont et Chaussees (ENPC)*, 351 p.

Benz Navarrete, M. A., Breul, P and Gourves, R. 2022. Application of wave equation theory to improve dynamic cone penetration test for shallow soil characterisation, *Journal of Rock Mechanics and Geotechnical Engineering*, Vol. 14, 289-302.

Chattaraj R. & Sengupta, 1. 2016. Liquefaction potential and strain dependent dynamic properties of Kasai River sand, *Soil Dynamics and Earthquake Engineering*, Vol.90, 467-475.

Francisković-Bilinski, S., Bhattacharya, A.K., Bilinski, H., Bhattacharya, B.K., Mitra, A. and Sarkar, S.K. 2011. Fluvial geomorphology of the Kupa River drainage basin, Croatia: A perspective of its application in river management and pollution studies*, Zeitschrift für Geomorphologie*, Vol. 56, 1, 93 -119.

Green R.A. & Terri G.A. 2005. Number of Equivalent Cycles Concept for Liquefaction Evaluations - Revisited, *Journal of Geotechnical. and Geoenvironmental Engineering*, 131(4): 477-488.

Hancock J. & Bommer J. J. 2005. The effective number of cycles of earthquake ground motion, *Earthquake Engineering & Structural Dynamics*, 34: 637-664.

Herak, D. & Herak, M. 2010. The Kupa Valley (Croatia) Earthquake of 8 October 1909 - 100 Years Later, *Seismological Research Letters,* Vol. 81 n°1, 30-36.

Hutabarat D. & Bray J.D. 2021. Estimating the Severity of Liquefcation Ejecta Using the Cone Pentration Test, *Journal of Geotechnical. and Geoenvironmental Engineering*, 148(3), 1-16.

Idriss I.M. & Boulanger R.W. 2008. Soil liquefaction during earthquakes. Earthquake *Engineering Research Institute*, Monograph MNO-12, Oakland, CA. 262 p.

International Organization for Standardization (ISO). 2023. Prebored pressuremeter test, Geotechnical investigation and testing - Field testing. ISO standard N°22476-5, 37 p.

Karagiannopoulos P.G., Dang Q. H. Reiffsteck P., Benoit J., Dupla J.-C., Peronne M. 2022. Multicycle expansion tests in natural soils, *European Journal of Environmental and Civil Engineering*, 27:1-18

Kokusho T. 2016. Major advances in liquefaction research by laboratory tests compared with in-situ behavior, Soil Dynamics and Earthquake Engineering, Vol. 91, 3-22.

Kramer, S.L. 1996. Geotechnical Earthquake Engineering, *Prentice-Hall, Englewood Cliffs NJ*, 653 p.

Lasley S.J., Green R. A. and Rodriguez-Marek A. 2016. Number of Equivalent Stress Cycles for Liquefaction. Evaluations in Active Tectonic and Stable Continental Regimes, *Journal of Geotechnical. and Geoenvironmental Engineering*, 143 (4), 1-11.

Lee, M.W. 2010. Predicting S-wave velocities for unconsolidated sediments at low effective pressure: *U.S. Geological Survey* Scientific Investigations Report 2010– 5138, 13 p. 11.

Luong T.A., Moiriat D., Reiffsteck P., et al., 2023. Use of the new dynamic cone penetrometer for the study of soil liquefaction along the Kupa River, Petrinja Area (Croatia), *Proceedings of the 9th Conference of Croatian Geotechnical Society*, Sisak, May 4- 6. 101-110.

Morrison M. J. 2017. Shallow Shear-Wave Seismic Analysis of Point Bar Deposits of False River, Louisiana, *Louisiana State University and Agricultural and Mechanical College LSU*, 127 p.

Pyke, R. 2003. Discussion of liquefaction resistance of soils: Summary report from the 1996 NCEER and 1998 NCEER/NSF workshops on evaluation of liquefaction resistance of soils. *Journal of Geotechnical. and Geoenvironmental Engineering*, 129(3), 283-284.

Reiffsteck P., Fanelli S., Tacita J.-L. 2013. Determining small strain elastic modulus using cyclic expansion tests, *Proceedings of the 18th International Conference on Soil Mechanics and Geotechnical Engineering*, Paris, 2383-2386

Retamales S. 2022. Development of a method to evaluate the risk of liquefaction of sands from a dynamic penetrometer test. Ph. D Thesis, *CERMES*, Ecole des Ponts ParisTech, 224 p.

Robertson P.K. & Wride C.E. 1998. Evaluating cyclic liquefaction potential using the cone penetration test, *Canadian Geotechnical Journal*, J. 35, 442-459.

Robertson P.K., 2009. Interpretation of cone penetration tests – a unified approach, *Canadian Geotechnical Journal*. J. 46, 1337–1355.

Robertson P.K. & Cabal K. 2022. Guide to Cone Penetration Testing, 7th Edition, *P.K. Robertson Consulting*, 163 p.

Seed, H. B., and Idriss, I. M. 1971. 'Simplified procedure for evaluating soil liquefaction potential, *Journal of the Geotechnical Engineering Division*, 97(9), 1249-1273.

Semple, R. 2013. Problems with liquefaction criteria and their application in Australia, *Australian Geomechanics*, Vol. 48, n°3, 15-48.

Serratrice J.F. 2016. Digues de Donzère. Essais de laboratoire, compte-rendu, *Ed. CEREMA*, Aix-en-Provence, 140 p.

Valkaniotis S., Rapti D., Taftsoglou M., Papathanassiou G. and Caputo R.. 2024. Geomorphological mapping for liquefaction likelihood: the Piniada case study (Central Greece), Bulletin of Earthquake Engineering 22: 5451-5474.

Youd T.L., Idriss I.M., Andrus R.D., et al.. 2001. Liquefaction resistance of soils: summary report from the 1996 NCEER and 1998 NCEER/NSF workshops on evaluation of liquefaction resistance of soils. *Journal of Geotechnical. and Geoenvironmental Engineering*, 127(10), pp 817-833.